41st AIAA/ASME/SAE/ASEE Joint Propulsion Conference and Exhibit
July 10–13, 2005/Tucson, AZ

Simulation of Detonation Propagation in Turbulent Gas-Solid Reactive Mixtures

Franklin Génin*, Bruce Fryxell† and Suresh Menon‡
Georgia Institute of Technology,
Atlanta, GA, 30332-0150,
USA

The present study focuses on the simulation of highly reactive two-phase flows associated with detonations. A hybrid scheme, that combines a high-order shock-capturing method and a second/fourth-order accurate, low dissipation scheme[1] is first validated by simulating blast wave discharges and shock-vortex interaction. The Large-Eddy Simulation model used in the present formulation is considered afterward in a fundamental study of shock-turbulence interaction. The solid phase tracking algorithm is then validated in supersonic environment. Finally, a detonative mixture composed of $H_2/O_2/Ar$, similar to an experimental configuration,[2] is simulated with and without the presence of solid aluminum particles. The explicit role of the particles in this environment is considered, and the presence of a $Double-Fronted\ Detonation$ is analyzed.

I. Introduction

Detonations in multi-phase (e.g. gas-solid) mixtures have been studied in the past, both experimentally and theoretically, in order to understand their initiation, propagation mechanism and their interaction with reactive turbulent flows. Such configurations have many practical applications. Detonations can be used for propulsion purpose, *e.g.*, in pulse-detonation engines. This type of studies can also be important for safety studies. Explosions in coal mines, for instance, are associated with the dispersion of coal dust from the mine walls by a passing pressure wave, so forming a highly reactive dust cloud.

Numerical simulations are a very efficient tool in order to obtain a fundamental understanding of such systems, since a controllable time resolution can easily be achieved. However, the problem is complex since many physical processes are involved, such as, phase transition, turbulent scalar mixing, strong shock propagation, and chemical reactions. A computational approach must be capable of resolving not only the mixing region, but also be able to capture the strong shock motion without excessive numerical diffusion.

To get an accurate simulation of such unsteady processes, where typical Reynolds number are high, and where turbulent motions have a significant influence on the overall process, Large-Eddy Simulation (LES) appears to be a viable option. However, conventional LES methods and models are not usually capable of capturing shock-shear interaction. Classical shock capturing methods are far too dissipative for shock-turbulence interactions, and as such, tend to dissipate the fine-scale turbulent structures in the flow. In this study, a recently developed LES approach,[1] that combines a high-order shock capturing algorithm within the LES framework (described in more details in section II) is used to study detonation in multi-phase environment. The scheme is first validated by simulating classical test problems, and then, the subgrid closure approach[3] validity is extended to supersonic flows computations. This general approach is finally used to study the process of metal particles ignition in a shock tube environment.

*Graduate Research Assistant, AIAA Student Member
†Senior Research Scientist, AIAA Member
‡Professor, and AIAA Associate Fellow

II. Governing Equations and Numerical Method

A. LES governing equations for the gas phase

The governing equations for LES are obtained by applying a spatial filter (based on the local grid size $\overline{\Delta}$) to the compressible Navier-Stokes equations for the mass, momentum, total energy, and species conservation. Favre averaging, commonly used in the study of compressible flow, and defined by $\widetilde{f} = \overline{\rho f}/\overline{\rho}$, where the over-line stands for volume averaging, is applied to obtain the resulting filtered LES equations.

$$\begin{cases} \frac{\partial \overline{\rho}}{\partial t} + \frac{\partial \overline{\rho} \widetilde{u_i}}{\partial x_i} = \widetilde{\dot{\rho}_s} \\ \frac{\partial \overline{\rho} \widetilde{u_i}}{\partial t} + \frac{\partial}{\partial x_j} \left[\overline{\rho} \widetilde{u_i} \widetilde{u_j} + \overline{p} \delta_{ij} - \overline{\tau_{ij}} + \tau_{ij}^{sgs} \right] = \widetilde{\dot{F}_{s,i}} \\ \frac{\partial \overline{\rho} \widetilde{E}}{\partial t} + \frac{\partial}{\partial x_i} \left[\left(\overline{\rho} \widetilde{E} + \overline{p} \right) \widetilde{u}_i + \overline{q_i} - \widetilde{u_j} \overline{\tau_{ij}} + H_i^{sgs} + \sigma_{ij}^{sgs} \right] = \widetilde{\dot{Q}_s} \\ \frac{\partial \overline{\rho} \widetilde{Y_k}}{\partial t} + \frac{\partial}{\partial x_i} [\overline{\rho} \tilde{Y}_k \tilde{u}_i - \overline{\rho} \tilde{Y}_k \widetilde{V_{i,k}} + Y_{i,k}^{sgs} + \theta_{i,k}^{sgs}] = \bar{\dot{w}}_k + \widetilde{\dot{S}_{s,k}} \qquad k = 1, N_s \end{cases} \tag{1}$$

where $\overline{\dot{\rho}^s}$, $\overline{F_i^s}$, $\overline{\dot{Q}^s}$ and $\widetilde{\dot{S}_{s,k}}$ are respectively, the source terms from the spray evaporation for mass, momentum, energy, and species, and $\bar{\dot{w}}_k$ is the production rate for species k, due to reaction.

A perfect gas assumption is used throughout this study. The non-reacting simulations use a calorically perfect gas assumption, whereas the shock-tube reactive configurations were simulated using a thermally perfect gas assumption. Both the viscosity and the thermal conductivity of the species were approximated by a Sutherland law. The heat flux term is written in the following form:

$$\bar{q}_i = -\bar{\kappa} \frac{\partial \tilde{T}}{\partial x_i} + \bar{\rho} \sum_{k=1}^{N_s} \tilde{h}_k \tilde{Y}_k \widetilde{V_{i,k}}.$$

The diffusion velocities are approximated using Fickian diffusion as $\widetilde{V_{i,k}} = (-\bar{D}_k / \tilde{Y}_k)(\partial \tilde{Y}_k / \partial x_i)$ where pressure diffusion (Dufour) and temperature diffusion (Soret) effects are neglected.

Several terms in the LES equations require closure. Here, a closure based on a transport model for the subgrid kinetic energy k^{sgs} is used to close the momentum and energy subgrid fluxes. In this approach, a one-equation model for k^{sgs}:

$$\begin{aligned} \frac{\partial \overline{\rho} k^{sgs}}{\partial t} + \frac{\partial}{\partial x_i} \left(\overline{\rho} \widetilde{u_i} k^{sgs} \right) &= \\ P^{sgs} - D^{sgs} &+ \frac{\partial}{\partial x_i} \left(\frac{\overline{\rho} \nu_t}{Pr_t} \frac{\partial k^{sgs}}{\partial x_i} \right) + F_k \end{aligned} \tag{2}$$

is solved along with the LES equations. Here, F_k is the work done due to the two-phase coupling force term $\dot{F_{s,i}}$, ν_t is the turbulent viscosity and Pr_t is the turbulent Prandtl number. P^{sgs} is the subgrid kinetic energy production, D^{sgs} is the subgrid kinetic energy dissipation. These terms are given by:

$$\nu_t = C_\nu \sqrt{k^{sgs}} \quad \overline{\Delta} \tag{3}$$

$$P^{sgs} = -\tau_{ij}^{sgs} \frac{\partial \widetilde{u_i}}{\partial x_j} \tag{4}$$

$$D^{sgs} = C_\epsilon \overline{\rho} \frac{\sqrt{(k^{sgs})^3}}{\overline{\Delta}} \tag{5}$$

The subgrid stresses and energy flux are closed as follows:

$$\tau_{ij}^{sgs} = -2 \overline{\rho} \nu_t \left(\widetilde{S_{ij}} - \frac{1}{3} \widetilde{S_{kk}} \delta_{ij} \right) + \frac{2}{3} \overline{\rho} k^{sgs} \delta_{ij} \tag{6}$$

$$H_i^{sgs} = -\overline{\rho} \frac{\nu_t}{Pr_t} \frac{\partial \widetilde{H}}{\partial x_i} \tag{7}$$

where $\widetilde{H}$ is the total enthalpy. The subgrid viscous work, σ_i^{sgs}, that appears in the filtered energy equation, is neglected, based on the earlier work of Kim *et al.*[4] In the above closure, two model coefficients C_ν and C_ϵ

appear. Constant values of 0.067 and 0.916 can be employed for these constants based on earlier evaluation of these parameters.[5]

A localized dynamic approach (LDKM) has also been developed[3] to compute these coefficients as a part of the solution. The fundamental idea behind this method consists in using the information at the resolved scale to compute the subgrid scale behavior by similarity relations. This method has been successfully used for both non-reacting[6,7] and reacting[4,8] flows. Nelson[9] found that well-resolved and fully turbulent simulations using this approach would satisfy the *realizability* constraints.

In the case of supersonic turbulent flows simulations however, where the compressibility can reach high values, and where shocks are to be correctly captured and simulated, an explicit *realizability constraint* has to be imposed to the computation of the c_ν coefficient. Following the approach given in Thivet *et al*, the new approach, called hereafter $LDKM_s$, reads:

$$c_\nu^{LDKM_s} = min\Big(c_\nu^{LDKM}, \frac{0.3C_\epsilon\sqrt{k^{sgs}}}{S\Delta}\Big) \tag{8}$$

where S is given by $S = 2(S_{ij}S_{ji} - \frac{1}{3}S_{kk})$. This approach is tested in the present study for the fundamental configuration of a shock/turbulence interaction.

B. Numerical method for the gas phase

The numerical approach used in the present study uses a hybrid method that couples a high-order finite-volume method with a high-resolution shock capturing algorithm. The shock capturing technique is used only near shocks and contact discontinuities, while the high-order method handles the smooth regions of the flow. The code used for this study is a well-established LES solver (LESLIE3D) developed for scalar mixing and combustion application in gas turbine and SCRAMJET engines.[4,10,11,12]

A shock capturing technique based on the Piecewise-Parabolic Method (PPM)[13] is combined with the existing finite-volume scheme (second or fourth-order) in the original LESLIE3D code.[14] The PPM algorithm is a high-order extension of the method originally developed by Godunov.[15] In PPM, the flow variables are represented as piecewise-parabolic functions. Although this could lead to a method which is accurate to third order, PPM is formally accurate to only second-order in both space and time. However, the most critical steps are performed to third-order or fourth-order accuracy, resulting in a method which is considerably more accurate and efficient than most second-order codes using typical grid sizes.

In the current implementation, we employ PPM only in regions where it is necessary and switch back to the high-order predictor-corrector scheme in LESLIE3D in regions where there are no strong discontinuities. This approach has been used in the past,[1] and showed good efficiency in simulating classical inviscid test-cases (Shu-Osher test problem, inviscid Richtmyer-Meshkov instability). Turbulent simulations using this hybrid method are presented in this paper.

C. Lagrangian phase algorithm

The treatment of the liquid phase is achieved using a Lagrangian approach, where particle groups are explicitly tracked throughout the domain. This approach is preferred to alternative Eulerian techniques, since it allows for an accurate description of the evaporation process, the gas/dense-phase coupling, and the actual motion of the particles. Two-way coupling between the gas and liquid phases is implemented. A detailed description of the approach, of its assumptions, and its limitations can be found elsewhere.[16] This approach has been used with success within the LESLIE3D approach for a wide range of applications.[10,17,18] Validation of the tracking method is presented in the present paper using the hybrid method.

The present study focuses on the combustion of aluminum (Al) particles in a shock tube, and thus, differs from previous simulations in the sense that solid particles are simulated, rather than liquid fuels. Some assumptions specific to this study are necessary, and are presented here.

It is widely known[19] that when an aluminum particle is exposed to a hot oxidizing low-speed flow, aluminum oxide (Al_2O_3) resulting from the combustion will create a cap around the particle, that will reduce the heat transfer from the flow to the particle and prevent the aluminum from evaporating. As a consequence, a decrease in the combustion efficiency is observed. In the present study, this condensation is neglected, under the assumption that the high convection of the flow will prevent the aluminum oxides from depositing on the surface of the particles. This assumption seems reasonable for the present study, where the shock-induced velocities and turbulence will be high. Future studies will revisit this issue.

The particles under consideration are solid at first. Rather than simulating the melting process of the particles, which would imply a dual Lagrangian tracking algorithm, it is chosen to treat the particles as one condensed phase, with a variable specific heat, that takes the latent heat of liquefaction into account. This assumption seems again reasonable, since the melting point of Aluminum is $1800K$ lower than its boiling point, so that no evaporation of the particles is expected at such temperatures.

D. Chemistry

1. Hydrogen/Oxygen chemistry

A seven-step mechanism is here adopted for the hydrogen chemistry. It is a modified version of the Spark model (originally developed by Jachimowski[20]), employed by Eklund, Drummond and Hassan.[21] The forward rates are given by:

$$\begin{array}{lllllllll} H_2 & + & O_2 & & & \rightarrow & OH & + & OH \\ O_2 & + & H & & & \rightarrow & OH & + & O \\ H_2 & + & OH & & & \rightarrow & H_2O & + & H \\ H_2 & + & O & & & \rightarrow & OH & + & H \\ OH & + & OH & & & \rightarrow & H_2O & + & O \\ OH & + & H & + & M & \rightarrow & H_2O & + & M \\ H & + & H & + & M & \rightarrow & H_2 & + & M \end{array} \qquad \begin{array}{ll} k_1 & = 1.70 \times 10^{13} e^{-24233/T} \\ k_2 & = 1.42 \times 10^{14} e^{-8254/T} \\ k_3 & = 3.16 \times 10^{7} T^{1.8} e^{-1525/T} \\ k_4 & = 2.07 \times 10^{14} e^{-6920/T} \\ k_5 & = 5.50 \times 10^{13} e^{-3523/T} \\ k_6 & = 2.21 \times 10^{22} T^{-2} \\ k_7 & = 6.53 \times 10^{17} T^{-1} \end{array} \tag{9}$$

The backward reaction rates were found using the thermodynamic equilibrium constants for each reaction. The Chaperon efficiencies for the two last reactions in the mechanism were implemented following the approach by Balakrishnan *et al*:[22] Chaperon efficiencies for the sixth reaction are $H_2 : 2.5$, $H_2O : 12$ and $O_2 : 1$, while for the last reaction, they are given by: $H_2 : 1$, $H_2O : 6.5$ and $O_2 : 0.4$.

2. Aluminum chemistry

The system under consideration is composed of aluminum particles exposed to high pressure/temperature by the effect of a traveling shock/detonation. Once the particles reach high internal temperature, the evaporation generates gaseous aluminum that will react with the ambient oxygen in the flow. The reactions considered in this study are based on the work of Beckstead.[19] First, the evaporation of the particles is considered, and a three-step reaction mechanism is used:

$$\begin{array}{lllllll} Al_l & & & \rightarrow & Al_g & & \\ Al_g & + & O_2 & \rightarrow & AlO & + & O \\ AlO & + & O_2 & \rightarrow & AlO_2 & + & O \\ Al_g & + & H_2O & \rightarrow & AlO & + & H_2 \end{array} \qquad \begin{array}{ll} k_8 & = 9.76 \times 10^{15} e^{-80/T} \\ k_9 & = 4.63 \times 10^{14} e^{-10008/T} \\ k_{10} & = 1.90 \times 10^{-12} e^{-443/T} \\ & \quad + 1.60 \times 10^{-10} e^{-2869/T} \end{array} \tag{10}$$

III. Validation of the approach

Some validation studies have been conducted, and presented in a previous paper.[1] Those tests focused on the validation of the hydrodynamic solver. Presented here are other validation cases that establish the capability of the hybrid scheme in both non-reacting and reacting mixtures, under viscous and turbulent conditions.

A. Simulation of Blast Wave Propagation

Direct Numerical Simulation of a blast wave diffraction on a backward facing step (of height H) is conducted using a PPM approach for the Euler equations, similar to the case presented by Liang and Chen.[23] This study serves to validate the PPM algorithm in the code. The blast wave is initiated by the creation of a pressure impulse over $0.01H$, at a distance of $0.525H$ upstream the face corner. The impulse being 72 times the ambient pressure, the blast wave so created reaches the corner with a Mach number of 1.5. A grid of 600×600 grid points is employed for this study.

Once released, the stripe of pressure impulse generates one moving shock on each side, each followed by a rarefaction fan. The expansion decreases the pressure below the local atmospheric pressure, and a secondary shock is created that brings the pressure back to atmospheric value. The whole process results in two traveling shock waves on each side of the initial pressure impulse.

The head shock interacts with the corner of the step, and the shock diffraction generates vorticity via baroclinic effect. The vorticity at the corner of the step, and its interaction with the secondary wave (see Fig. 1) are correctly simulated, and the shock is captured very crisply. Also, the Mach number of the diffracted wave, along the back face of the step, is measured to be 1.13, while the experimental value for this blast wave Mach number as reported by Liang *et al*[23] is of 1.15.

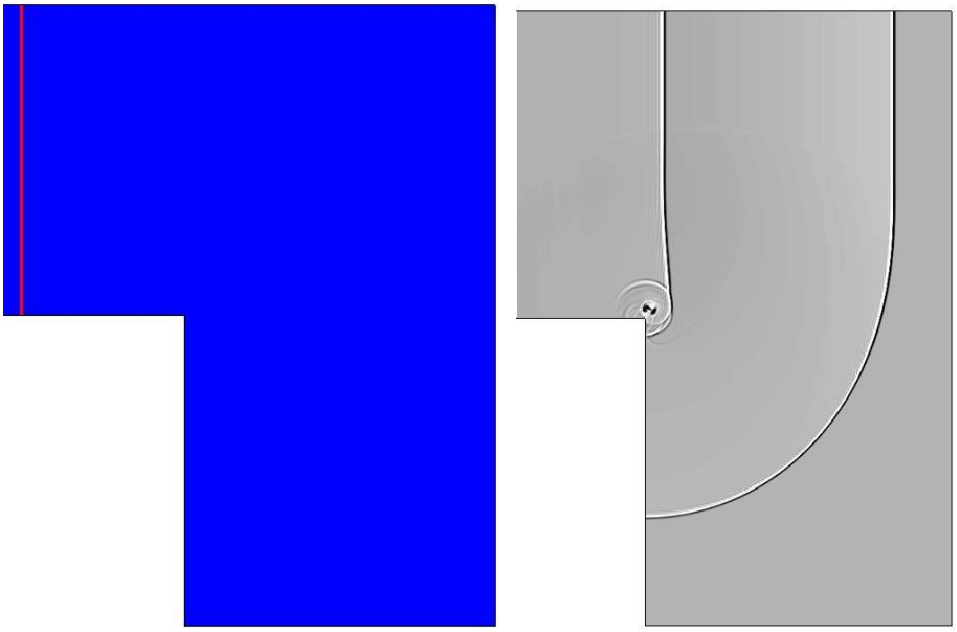

(a) Initial conditions - thin region of overpressure

(b) Secondary shock / vortex interaction

Figure 1. Blast wave diffraction at a sharp corner. (a): Initialization of a high pressure region upstream the corner. (b): Numerical shadowgraph of the interaction of the secondary shock with the vortex generated by the first shock diffraction - shadowgraph image, *i.e.* $\nabla^2\rho$**.**

B. Validation of the scheme for simulating high-speed turbulent flows

The fundamental assumption of LES is that the small scales are universal, and that only the large scales are flow dependent. An efficient scheme should thus minimize the numerical dissipation, and adopt an accurate subgrid closure model. In this section, the applicability of the current LES scheme to the simulation of high-speed turbulent flow will be demonstrated.

First, the ability in simulating the large scales is studied. Vortical coherent structures are inherent features of turbulent flows. A simulation is conducted that shows that the presented scheme provides accurate results for the large scales of turbulence. Subsequently, the model for the small scales is tested by simulating a turbulence/shock interaction configuration.

1. Shock/Vortex Interaction

A vortex convected towards a shock is chosen for validation purposes. Linearized models of vorticity amplification through shocks have been developed,[24] that state that the ratio between post- and pre- shock

maximum vorticity scales as the ratio between post- and pre- shock mean densities:

$$\frac{\omega_2}{\omega_1} = \frac{\rho_2}{\rho_1} \tag{11}$$

A two dimensional simulation is performed, where a Mach 1.7 mean flow convects a single vortex through a normal stationary shock. Under those conditions, the density ratio is 2.19. The vortex is defined by:

$$v_r(r) = 0. \tag{12}$$

$$v_\theta(r) = v_{max}\frac{r}{R}e^{\frac{1}{2}(1-\frac{r^2}{R^2})} \tag{13}$$

$$\frac{d\ P(r)}{d\ r} = \rho(r)\frac{v_\theta^2(r)}{r} \tag{14}$$

$$\frac{P(r)}{\rho^\gamma(r)} = const. \tag{15}$$

These relations fully define the vortex flowfield. Integrating these equations leads to a pressure profile:

$$P(r) = P_0\left(1 - \frac{\gamma-1}{2}M_v^2 e^{1-\frac{r^2}{R^2}}\right)^{\frac{\gamma}{\gamma-1}} \tag{16}$$

where M_v is the stagnation-based maximum Mach number in the vortex: $M_v = v_{max}/a_0 = v_{max}/\sqrt{\gamma P_0/\rho_0}$, and is set to 0.2 for the present study. This profile is superimposed onto a mean convecting flow, with a static pressure P_0, a static density ρ_0, and a mean velocity $U_{mean} = 1.7 \quad a_0$. A grid with 600×200 uniformly distributed points is used to perform this simulation, and 20 grid points are used to resolve one radius R of the vortex. Snapshots of the vortical field for this simulation, as well as the time evolution of the normalized maximum vorticity are presented in Fig. 2, where t_{inter} denotes the time of first interaction between the vortex and the shock front. The maximum vorticity trace shows a sudden increase when the vortex impinges the shock. The counter-rotating velocity fields result in the corrugation of the shock front. During the period of time when the vortex is passing through the shock, the maximum vorticity is not contained within the vortex, but appears at its edges, where the shock is being distorted. This region is delimited by dotted lines, and is not to be considered.

After the vortex has passed through the shock, it is observed that its vorticity ratio stabilizes at a value very close to the linear theory prediction. Also, it can be seen that a precessing motion of the vortex occurs after the interaction has occurred. This phenomenon is explained by the baroclinic effect of the shock corrugation on the vortex center. The distortion of the shock is a non-linear process, such that the shock front corrugation is non anti-symmetric, thus generating a pressure gradient that does not align with the vortex density gradient. Torque is thus created during the interaction.

2. Shock/Turbulence Interaction

It is well known, from analytical studies in the early 1950s and experimental evidence in the 1980s, that the effect of a shock on homogeneous turbulence is to increase the level of turbulence in the post-shock region. This is partly attributed to the increase in the vorticity mode through the shock. With the development of high-order upwind schemes, many Direct Numerical Simulations of shock-turbulence interaction have been recently conducted.[25,24,26]

The application of RANS/LES simulations to such flows is even more recent, and a few researchers have simulated this type of flows with success. Sinha *et al*[27] used this test case to develop an improved closure model for RANS simulations, and were able to get the right increase in the level of turbulence and decay rate in the post-shock region. The near shock behavior, however, did not show the right trend. LES have also been performed,[28,29] and showed good capturing of both near and far shock regions. This case is good as a test case for the accuracy of a shock capturing high order scheme, and for the validity of a LES closure model in compressible simulations.

The configuration adopted in the present study is similar to case $1.29A$ by Mahesh *et al*.[24] The fluid is assumed to be a perfect gas. A Prandtl number of 0.76, and a power-law viscosity $\mu \approx T^n, \quad n = 0.76$ are assumed.

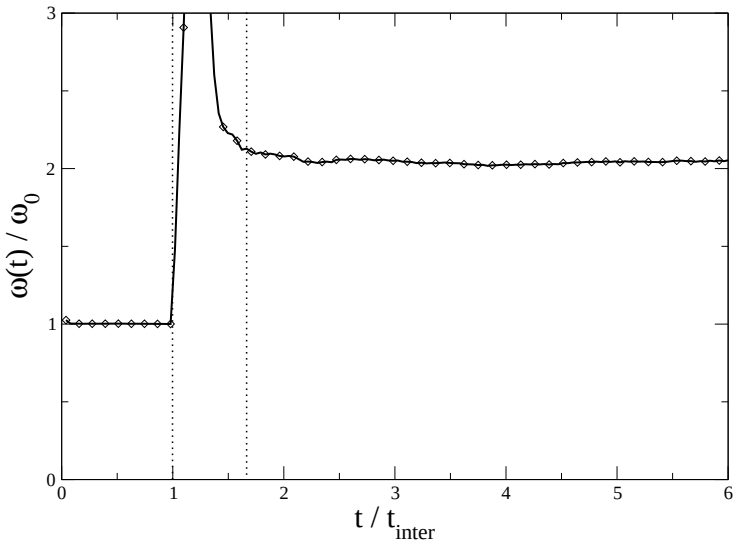

(a) Temporal evolution of the maximum vorticity

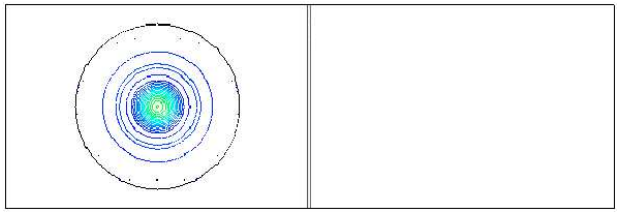

(b) t = 0

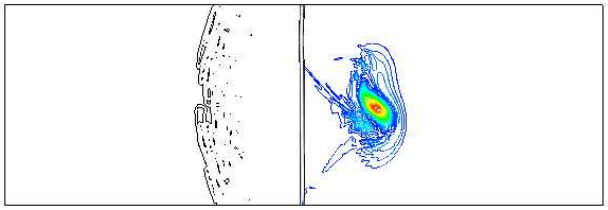

(c) t = $1.5 \times t_{inter}$

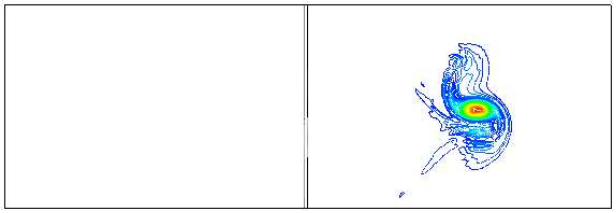

(d) t = $2 \times t_{inter}$

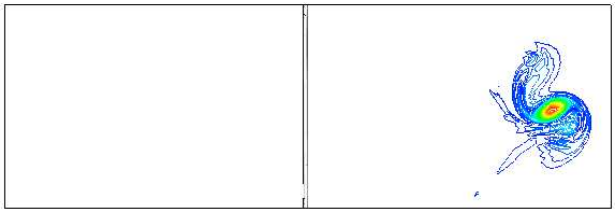

(e) t = $2.5 \times t_{inter}$

Figure 2. Shock-vortex interaction: (a) Evolution of the maximum vorticity normalized by its initial value with time (b)-(e): Snapshots of the vorticity field during shock-vortex interaction.

A temporal simulation of compressible decaying turbulence in a $(8\pi/k_0)^3$ cubic box (where k_0 is the most energetic wavenumber at the initialization), using $32 \times 32 \times 32$ grid points, is first conducted to generate a physical turbulent field that is to be used at the inflow of the spatial simulation.

The initial velocity field of the temporal simulations has an energy spectrum that satisfies:

$$E(k) = 16\sqrt{\frac{2}{\pi}}\frac{u_{rms}^2}{k_0}\Big(\frac{k}{k_0}\Big)^4 exp\Big[-2\Big(\frac{k}{k_0}\Big)^2\Big] \tag{17}$$

The other initial parameters are given by a Taylor micro-scale Reynolds number $Re_\lambda = u_{rms}\lambda/\bar{\nu} = 39.5$ and a turbulent Mach number $M_t = |q|/\bar{c} = 0.22$. No thermodynamic fluctuations are imposed at the

initialization. This simulation is conducted until the Taylor micro-scale Reynolds number reaches a value of $Re_\lambda = 19.1$. The turbulent Mach number at this final stage is equal to 0.14, similarly to the results obtained by Mahesh *et al.*

A mean velocity is then added to the perturbed field obtained from the temporal simulation, and this is used as inflow conditions for the spatial simulation. The domain, of dimensions $((8\pi + 4)/k_0)(8\pi/k_0)^2$, is resolved using $62 \times 32 \times 32$ grid points. In comparison, the DNS[24] employed $231 \times 81 \times 81$ grid points. A $M = 1.29$ shock is initialized using the normal shock relations at $k_0.x = 9$. Supersonic inflow is imposed, while characteristics based outflow[30] are used in the subsonic post-shock region. Periodicity conditions are imposed in both span- and cross- directions.

The simulation is run for two flow-through-times for the flow to settle down, and then, statistics were obtained over two more flow-through-times. 1-D profile of the longitudinal averaged Reynolds stresses are shown in Fig. 3, where the angled brackets denote average over spanwise, crosswise directions, and time.

$$\langle f(x) \rangle = \frac{1}{T}\frac{1}{L_y}\frac{1}{L_z}\int_0^T \int_{-l_y/2}^{l_y/2}\int_{-l_z/2}^{l_z/2} f(x,y,z,t)\ dz\ dy\ dt \tag{18}$$

The longitudinal Reynolds stress for the LES simulation is computed as:

$$R_{xx} = \langle U^2 \rangle - \langle U \rangle^2 + \frac{2}{3}k^{sgs} \tag{19}$$

The normalization of these quantities is achieved according to the pre-shock values. A region delimited by two dashed lines corresponds to the fluctuations of the shock front, which results in big fluctuations in the streamwise velocity. this fluctuation is not to be regarded as turbulent features. The corrugation of the shock front also produces fluctuations in the crosswise velocity. For turbulence considerations, this region is not to be considered.

The hybrid scheme used in the present paper is a blend of two high order methods. Simulations were first conducted in order to test each one of these methods independently, by using both the LESLIE3D predictor/corrector base method and the PPM method by themselves, and results are presented in figure 3(a). The predictor/corrector centered scheme generates spurious oscillations, due to known odd/even decoupling, in the near shock region. This results first in a broadening of the shock front, and second, in non-physical apparent velocity fluctuations. Consequently, the turbulence statistics overshoot the DNS data.

The PPM approach, on the other hand, shows a very good capturing of the shock. The post-shock turbulence, however, is not correctly captured. The peak value of the streamwise turbulence is under estimated, and the decay rate is off.

The next step consists in using the predictor/corrector approach away from the shock only. Two methods are presented here. The first method consists in adding a classical *artificial dissipation* to the scheme,[31] that turns on in the regions close to the shock only, and that keeps the original scheme away from it.

The second method is the hybrid scheme, that uses PPM in the near-shock region, while smoothly switching to the predictor/corrector scheme away of it. Results of these simulations are presented in figure 3(b).

The *artificial dissipation* simulation shows a good capture of the post-shock region, with accurate prediction of the peak value. However, the pre-shock and post-shock turbulence decay are slightly over-predicted. This method acts like an extra viscosity, for scheme stability purpose. The lack of physical justification of this method leads to a lack of control on turbulent simulations. More particularly, a higher Mach number simulation might need more constraining dissipation coefficient for an efficient shock capturing property, thus leading to too high an extra dissipation.

The hybrid scheme approach, on the other hand, combines good shock capturing to the predictor/corrector scheme, and leads to an accurate representation of both regions, as can be observed in Fig. 3(b). The peak value of the post-shock turbulence appears very slightly over-estimated when $LDKM$ is used. The decay rate on both sides of the shock, on the other hand, is correctly captured.

As mentioned in section II A, the dynamic computation of the closure coefficients without the *realizability condition* can lead to an unphysical high value of the c_ν coefficient, especially in regions close to the shock. Adding the *realizability condition* improves these results: the peak value matches the DNS data, and the decay rate is correctly simulated. We therefore, consider the $LDKM_s$ as the new subgrid closure for flows with shock-shear interactions.

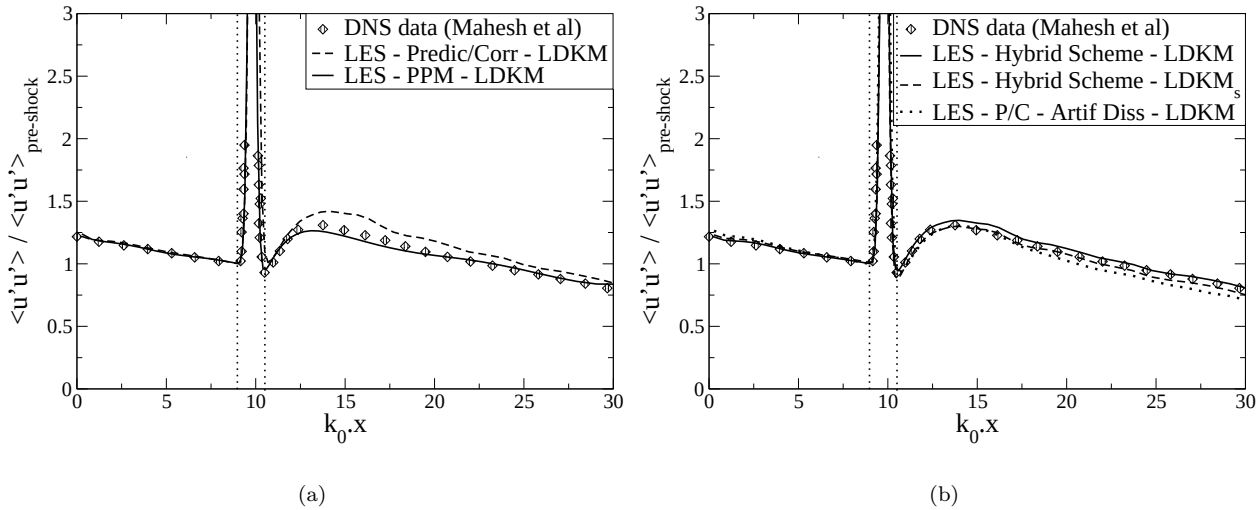

Figure 3. Comparison of the longitudinal Reynolds stresses for DNS and LES for the shock-turbulence interaction case

C. Particle Motion through a Shock

The Lagrangian tracking algorithm is tested by considering the relaxation time of particles passing through a weak shock. This is simulated for conditions similar to the experimental conditions presented by Tedeschi *et al.*[32] Here, particles with a diameter of $1.4\mu m$ are entrained in a $M = 2.3$ air flow, with a stagnation pressure of 0.5 $atm.$ and a stagnation temperature of $303K$. A shock is created by a 8 degrees ramp. The simulation is performed using PPM methods in a 2-D approach, using 60×30 grid points. Figure 4 shows the velocity profiles for the gas phase, the solid phase out of the computation, and the experimental results. It can be seen that the response of the particles to the sudden velocity change is well simulated.

As noted in Tedeschi *et al*,[32] the formulation of the drag coefficient used in this study:

$$C_D = \begin{cases} \frac{24}{Re_d}(1 + \frac{1}{6}Re_d^{2/3}) & for \quad Re_d \leq 1000 \\ 0.424 & for \quad Re_d > 1000 \end{cases}$$

where Re_D is the Reynolds number based on the slip velocity and the diameter of the particle, is only valid in the continuum regime, where the diameter of the particles is significantly bigger than the mean free path of the molecules composing the surrounding gas. This is verified in most of the industrial and atmospheric multiphase applications, and more particularly, this is verified in the present simulations.

IV. Detonation wave in a multiphase medium

A study on the effect of non-reacting and reacting particles on a detonation wave is presented here. It has been observed experimentally that the presence of particles in a reactive medium could lead to different detonative regimes. In particular, a phenomenon called $Double - Fronted\ Detonations$ has been observed when small reactive particles are added to a reactive mixture. Multiple-front detonations have also been recently reported. Those phenomena have been attributed to a combustion of the particles delayed from the detonation reaction region.

Very recently, a very similar phenomenon has been observed when seeding such reactive flows with inert particles,[2] in which case, the combustion of the particles cannot be the cause of this $Double-Shock$ structure, and the relevance as well as the physical cause of this phenomenon has been questioned by Carvel *et al.*[2]

Subsequently, the configuration under consideration is chosen to be similar to the experimental study conducted by Carvel *et al*,[2] where a detonation is initiated in a mixture of $2H_2 + O_2 + 3Ar$, originally at 26 kPa. In the present approach, only a portion of the shock-tube experiment is simulated, keeping,

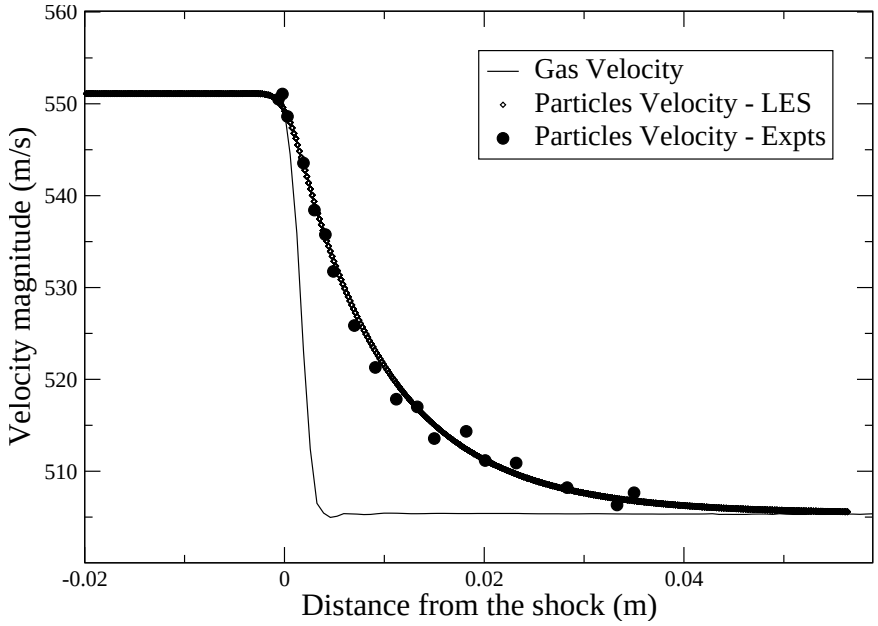

Figure 4. Comparison between numerical simulation and experiment for particle motion through a shock.

however, the particles mass loading similar to the experiments. The particles used in the experiments were 15 μm Al particles. Two mass loadings were tested, and both resulted in the same trends for the pressure traces. The particles mass loading tested in the experiments, and chosen for the present simulation, is of 20 g/m^3. The 7-step / 7 species mechanism described in Sec.II is directly integrated in order to resolve the chemical reactions. The initiation of the detonation is achieved by imposing a region of over-pressure at one end of the quiescent shock tube. The blast wave so-generated soon turns into a detonation.

A case of detonation without any particle is first simulated as a reference case. The second case considered here simulates evaporating aluminum particles, with the reaction mechanism for Aluminum described in Sec.II. The interaction between gas and solid phases being a complex phenomenon, some simulations are then presented to try and isolate the cause of the observed *double peak*.

Pressure traces have been collected during these simulations at two points, 0.7 m and 1.04 m downstream the ignition point. The profiles are represented in Fig. 5.

Gaseous detonation - no particles

The first case of detonation is performed to validate the chemistry used in this study. It is found that the detonation front travels at a speed of 1892 m/s in the current simulation, and a temperature of about 3200 K past the reaction zone of the detonation is reached. The Chapman-Jouguet point for this system corresponds to a front speed of 1877 m/s and a temperature of 3194 K.

Multiphase detonation - evaporating and reacting particles

The pressure profile shows a sharp re-compression after the strong decay region. This feature is observed in lieu of the second shock observed during the experiments. The location of this re-compression with respect to the detonation front extends in a first period of time, and then stabilizes to the separation observed in the second pressure trace, in Fig. 5.

In this simulation, the Al particles were acting as local heat sinks, absorbing some of the heat generated by the reaction, and heating up until they start evaporating. The heat exchange with the particles acts like an energy loss to the gas, thus generating pressure losses in the post-shock region. In the same time, the $slip - velocity$ of the particles (difference in velocity between the particle and the mean flow surrounding the particle under consideration) gets very high values in the post-shock region, thus generating a high drag

on the particles. The friction of the particles on the mean flow will result in a pressure loss, that tends to diminish as the particles get entrained by the flow.

Accordingly, a strong decay of the pressure is observed in the post wave region, and consequently, the detonation is seen to propagate at a slower speed than in the particle-less case. The front speed in this second case is of 1820 m/s.

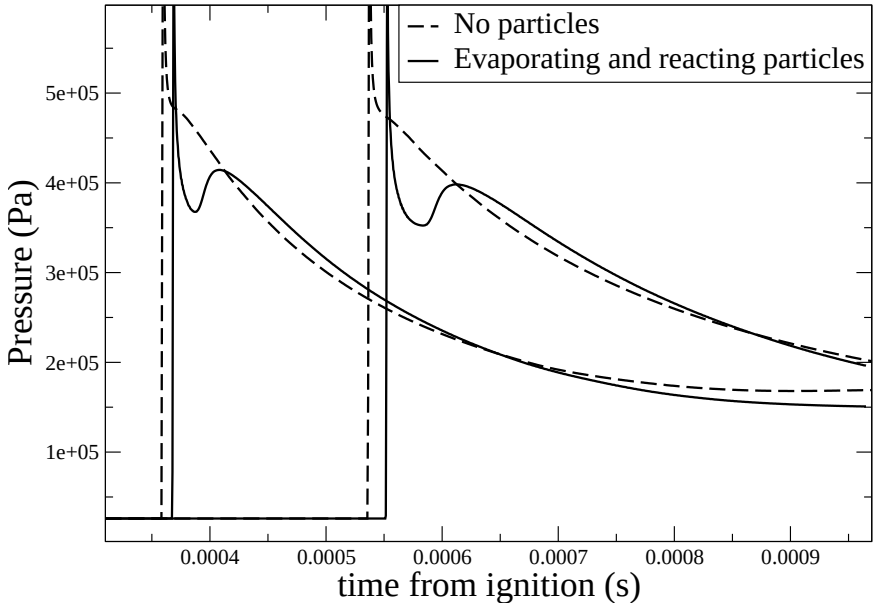

Figure 5. Pressure profiles collected $0.7\ m$ **and** $1.04\ m$ **downstream the ignition point. Two reference cases of detonations: no particles and evaporating/reacting particles**

In order to analyze the contribution of the friction of the particles, the heat exchange and mass exchange separately, the coupling parameters between the gas and solid phases are artificially fixed in the following simulations. The pressure profiles collected at the second station are represented in Fig. 6 for these three cases along with the simulations of pure gaseous and fully-coupled dual-phase detonations.

Gaseous detonation - particles with friction only

The case where inert particles are added to the flow and where the heat exchange between gas and solid phases is turned off is first considered to study the effect of the friction of the particles on the detonation wave. This case will later be referred to as the $non-calorific\ particles$ case. The very low mass loading of the particles is such that the effect of the particles appears to be negligible on the overall shape of the detonation. Hardly any delay is observed between the two detonations. A higher loading was observed to result in important pressure losses in the post-shock region. However, in the present case, no fundamental changes can be attributed to the drag of the particles on the flow.

Multiphase detonation - evaporating but non-reacting particles

A simulation is performed where the aluminum particles were evaporating, but the chemistry for aluminum is turned off. The effect of the particles on the gas phase starts in a very similar fashion as for the reacting case: a strong decay in the pressure is observed in the post-reaction region, due to the absorption of energy by the particles. In the non-reacting case, a re-compression is also observed to occur within some distance from the detonation front. Its amplitude is slightly lower than the one for reacting particles. Contrary to the reacting case, this feature is not stable, and is observed to decay further downstream, both in terms of physical location and of amplitude.

Thus, the pressure decay behind the detonation front is to be attributed to the heat absorption by the particles. The re-compression, on the other hand, is still very high even without reaction, and the influence of the mass exchange is next studied.

Multiphase detonation - non-evaporating calorific particles

For the next simulation, the heat exchange between particles and gas phase remains untouched, only the mass addition to the flow is suppressed. Again, the pressure losses in the post-front region are unchanged. The re-compression is still visible, but very low in amplitude, and decays at a fast rate.

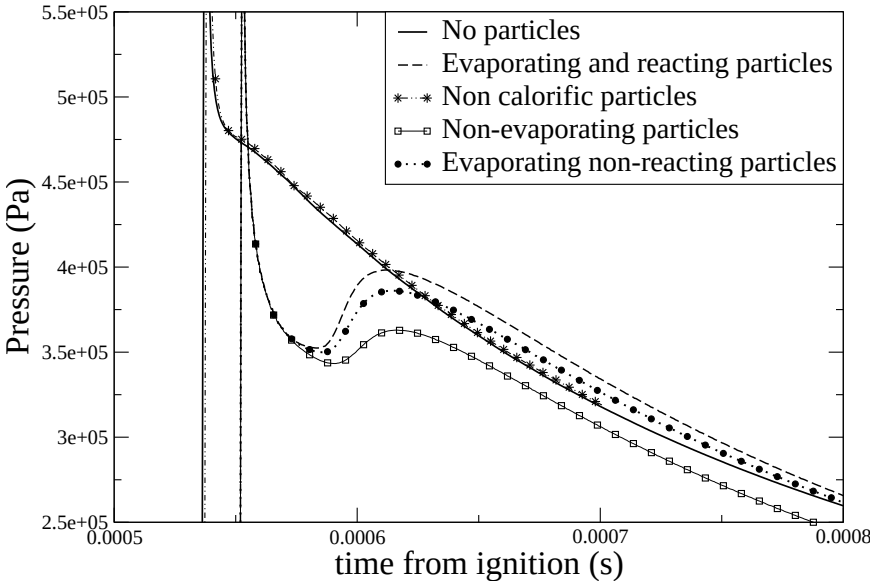

Figure 6. Pressure profiles collected $1.04\ m$ **downstream the ignition point. Two reference cases of detonations: no particles and evaporating/reacting particles. Three cases of partially-coupled detonations simulations: non-calorific inert particles, non-evaporating particles and evaporating/non-reacting particles**

It appears clearly from the present simulations that the strong decay in pressure, observed when particles are added to a detonative system, is mainly due to the energy exchange between gas and dense phases. The re-compression that occurs shortly after the detonation is probably a feature that is initialization-dependent for the most general case. In the case of burning particles, this secondary shock can be self-sustaining, while suppressing the reaction for particles results in a progressive suppression of this secondary compression. It has been specifically proven that the mass exchange due to the evaporation of the particles, coupled to the particles reaction, is for the main part responsible for sustaining the re-compression. However, particles reaction is necessary for the secondary shock to sustain.

V. Conclusion

A recently developed scheme, that incorporates a high-order shock-capturing method and a low-dissipation high order numerical discretization has been validated for simulations for flows containing both shock propagation and shear turbulence. Shock-vortex interaction and shock-turbulence interaction were simulated in order to show the ability of the new solver to resolve both large and small scales of a turbulent flow. A Lagrangian particle tracking/evaporating algorithm is then used and validated in terms of momentum exchange between gas and solid phases.

This numerical tool is applied to study the complex problem of $Double-Fronted\ Detonations$ with inert particles. It is shown that the $Double-Front$ observed in some experiments could be a misleading feature of the initial condition and of the set-up, since those features are not observed to be in a stable condition. The mechanisms that lead to a sustained $double-shock$ feature are isolated and analyzed. The appearance of this feature when inert particles are used appears to be a transient gas dynamic effect.

Acknowledgments

This work is supported in part by the Air Force Office of Scientific Research, the Office of Naval Research and the Eglin Airforce Base.

References

[1]Fryxell, B. and Menon, S., "Large-Eddy Simulation of Richtmeyer-Meshkov Instability." *AIAA Paper 2005–0314*, 2005.

[2]Carvel, R. O., Thomas, G. O., and Brown, C. J., "Some Observations of Detonation Propagation through a gas containing dust particles in suspension," *Shock Waves*, Vol. 13, 2003, pp. 83–89.

[3]Kim, W.-W. and Menon, S., "A New In-compressible Solver for Large-Eddy Simulations," *International Journal of Numerical Fluid Mechanics*, Vol. 31, 1999, pp. 983–1017.

[4]Kim, W.-W., Menon, S., and Mongia, H. C., "Large Eddy Simulations of a Gas Turbine Combustor Flow," *Combustion Science and Technology*, Vol. 143, 1999, pp. 25–62.

[5]Chakravarthy, V. and Menon, S., "Large-Eddy Simulations of Turbulent Premixed Flames in the Flamelet Regime," *Combustion Science and Technology*, Vol. 162, 2001, pp. 175–222.

[6]Menon, S., Yeung, P.-K., and Kim, W.-W., "Effect of Subgrid Models on the Computed Interscale Energy Transfer in Isotropic Turbulence," *Computers and Fluids*, Vol. 25, No. 2, 1996, pp. 165–180.

[7]Patel, N., Stone, C., and Menon, S., "Large-Eddy Simulation of Turbulent Flow over an Axisymmetric Hill," *AIAA Paper 2003–0967*, 2003.

[8]Kim, W.-W. and Menon, S., "Numerical Modeling of Turbulent Premixed Flames in the Thin-Reaction-Zones Regime," *Combustion Science and Technology*, Vol. 160, 2000, pp. 119–150.

[9]Nelson, C. C., *Simulations of spatially evolving compressible turbulence using a local dynamic subgrid model*, Ph.D. thesis, Georgia Institute of Technology, Atlanta, GA, December 1997.

[10]Sankaran, V. and Menon, S., "LES of Spray Combustion in Swirling Flows," *Journal of Turbulence*, Vol. 3, No. 11, 2001.

[11]Génin, F., Chernyavsky, B., and Menon, S., "Large Eddy Simulation of Scramjet Combustion Using a Subgrid Mixing/Combustion Model." *AIAA Paper 2003–7035*, 2003.

[12]Sankaran, V., Génin, F., and Menon, S., "A Sub-Grid Mixing Model for Large Eddy Simulation of Supersonic Combustion." *AIAA Paper 2004–0801*, 2004.

[13]Colella, P. and Woodward, P., "The Piecewise-Parabolic Method for Hydrodynamics," *Journal of Computational Physics*, Vol. 54, 1984, pp. 174.

[14]Menon, S., Fryxell, B., Stone, C., and Masquelet, M., "Direct Simulation of Solid Propellant Combustion and LES of High Energetic Detonation," *Computational Combustion Lab Technical Report, CCL-TR-04-023, September, 2004*, 2004.

[15]Godunov, S. K., "A Finite Difference Method For The Computation of Discontinuous Solutions of The Equations Of Fluid Dynamics," *Mat. Sbornik*, Vol. 47, 1959, pp. 357–393.

[16]Faeth, G. M., "Mixing, transport and combustion in sprays," *Progress in Energy and Combustion Science*, Vol. 13, 1987, pp. 293–345.

[17]Sankaran, V. and Menon, S., "Vorticity-scalar alignments and small-scale structures in swirling spray combustion," *Proceedings of the Combustion Institute*, Vol. 29, 2003, pp. 577–584.

[18]Génin, F. and Menon, S., "LES of Supersonic Combustion of Hydrocarbon Spray in a SCRAMJET," *AIAA Paper 2004–4132*, 2004.

[19]Beckstead, M. W., "A Summary of Aluminum Combustion," *paper presented at the RTO/VTI Special Course on Internal Aerodynamics in Solid Rocket Propulsion, 21–23 May 2002*, 2002.

[20]Jachimowski, C. J., "An Analytical Study of the Hydrogen-Air Reaction Mechanism with Application to Scramjet Combustion," *NASA TP 2791*, 1988.

[21]Eklund, D. R., Drummond, J. P., and Hassan, H. A., "Calculation of supersonic turbulent reacting coaxial jets," *AIAA Journal*, Vol. 28, No. 9, 1990, pp. 1633–1641.

[22]Balakrishnan, C., Trees, D., and Williams, F. A., "An Experimental Investigation of Strain-Induced Extinction of Diluted Hydrogen-Air Counterflow Diffusion Flames," *Combustion and Flame*, Vol. 98, No. 1, 1994.

[23]Liang, S. M. and Chen, H., "Flow Visualization of Numerically Simulated Blast Waves Discharging from Open-Ended Duct," *AIAA Journal*, Vol. 41, No. 12, 2003.

[24]Mahesh, K., Lele, S. K., and Moin, P., "The influence of entropy fluctuations on the interaction of turbulence with a shock wave," *Journal of Fluid Mechanics*, Vol. 334, 1997, pp. 353–379.

[25]Lee, S., Lele, S. K., and Moin, P., "Direct Numerical Simulation of Isotropic Turbulence Interacting with a Weak Shock Wave," *Journal of Fluid Mechanics*, Vol. 251, 1993, pp. 533–562.

[26]Lee, S., Lele, S. K., and Moin, P., "Interaction of Isotropic Turbulence with Shock Waves: Effect of shock Strength," *Journal of Fluid Mechanics*, Vol. 340, 1997, pp. 225–247.

[27]Sinha, K., Mahesh, K., and Candler, G. V., "Modeling shock unsteadiness in shock/turbulence interaction," *Physics of Fluids*, Vol. 15, No. 8, 2003, pp. 2290–2297.

[28]Ducros, F., Ferrand, V., Nicoud, F., Weber, C., Darracq, D., Gacherieu, C., and Poinsot, T., "Large-Eddy Simulation of the Shock/Turbulence Interaction," *Journal of Computational Physics*, Vol. 152, 1999, pp. 517–549.

[29]Garnier, E., Sagaut, P., and Deville, M., "Large Eddy simulation of shock/homogeneous turbulence interaction," *Computers & Fluids*, Vol. 31, 2002, pp. 245–268.

[30]Poinsot, T. and Lele, S., "Boundary Conditions for Direct Simulations of Compressible Viscous Flow," *Journal of Computational Physics*, Vol. 101, 1992, pp. 104–129.

[31]Jameson, A. and Liu, F., "Numerical Solution of the Euler Equations by Finite Volume Methods Using Runge-Kutta Time Stepping Schemes," *AIAA 81-1259*, 1981.

[32]Tedeschi, G., Elena, M., and Gouin, H., "Particle motion through an oblique shock wave," *Proceedings of SPIE - The International Society for Optical Engineering*, Vol. 2052, 1993.